Plug and Play DC-DC Converters for Smart DC Nanogrids with Advanced Control Ancillary Services

Guangyuan Liu, Aram Khodamoradi, Paolo Mattavelli, Tommaso Caldognetto, Paolo Magnone
Dept. of Management and Engineering (DTG), University of Padova, Italy
Email: guangyuan.liu@phd.unipd.it, aram.khodamoradi@phd.unipd.it, paolo.mattavelli@unipd.it, tommaso.caldognetto@unipd.it, paolo.magnone@unipd.it

***Abstract*—This paper gives a general view of the control possibilities for dc-dc converters in dc nanogrids. A widely adopted control method is the droop control, which is able to achieve proportional load sharing among multiple sources and to stabilize the voltage of the dc distribution bus. Based on the droop control, several advanced control functions can be implemented. For example, power-based droop controllers allow dc-dc converters to operate with power flow control or droop control, whether the hosting nanogrid is operating connected to a strong upstream grid or it is operating autonomously (i.e., islanded). Converters can also be equipped with various supporting functions. Functions that are expected to play a crucial role in nanogrids that fully embrace the plug-and-play paradigm are those aiming at the monitoring and tuning of the key performance indices of the control loops. On-line stability monitoring tools respond to this need, by continuously providing estimates of the stability margins of the loops of interest; self-tuning can be eventually achieved on the basis of the obtained estimates. These control solutions can significantly enhance the operation and the plug-and-play feature of dc nanogrids, even with a variable number of hosted converters. Experimental results are reported to show the performance of the control approaches.**

***Index Terms*—dc nanogrids; dc-dc converters; droop control; seamless transition; on-line stability monitoring.**

I. Introduction

Distributed Energy Resources (DERs) have been drawing more and more attention from both research and industry fields. DERs consist of distributed generators (DGs), which are typically based on renewable sources (e.g., photovoltaic, wind), and energy storage systems (ESSs) (e.g., batteries, super capacitors). Different kinds of DERs and local customers loads can be grouped in nanogrid [1]. Due to the dc nature of many DERs and loads, dc nanogrids show a more direct compatibility than their ac counterparts. The advantages of dc nanogrids include higher system efficiency, which is achieved by reducing dc-ac and ac-dc conversion stages, and simpler control strategies, because frequency and reactive power control issues are not present [2]. Generally, dc nanogrids can be linked to upstream grids (e.g., the utility, higher-level dc microgrids), increasing the flexibility of energy management. An example of dc nanogrid of generic layout is shown in Fig. 1.

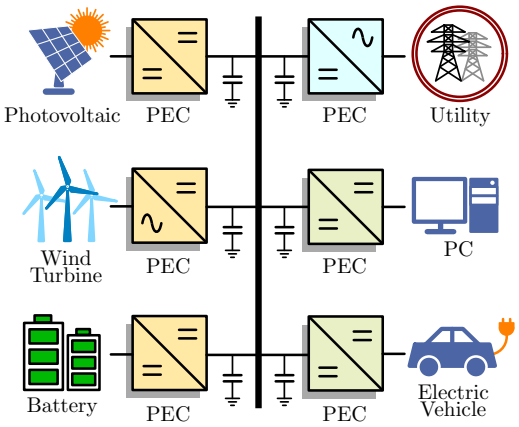

Figure 1. Example of a generic dc nanogrid.

In a dc nanogrid, the DERs and the upstream grids are interfaced with the common dc bus by DERs converters, most of which are dc-dc converters, and Grid-Interface Converters (GICs), respectively. Indeed, these converters serve as key components that give the possibility of performing various control functions, supporting a *smart* nanogrid. There are two main control objectives of DERs converters in dc nanogrids: *a)* regulating the power exchanged with the nanogrid; *b)* stabilizing the dc bus voltage and to balance the power within the nanogrid. Since these two goals are in conflict, each DERs converter can operate to fulfill only one of the two at a time. Droop control is a well-known solution for the case of multiple DERs converters connected to a common dc bus. In particular, it concurrently achieves bus voltage regulation and automatic load distribution [3]. With droop control applied, the load power is dispatched to DERs converters in inverse proportion to the droop coefficients, and the bus voltage varies in a predefined range as the total nanogrid load changes. Droop control can be implemented in different ways, thus attaining different control properties [4]. This part will be further addressed in the following section.

This work has received funding from the Electronic Components and Systems for European Leadership Joint Undertaking under grant agreement No 737434. This Joint Undertaking receives support from the European Union's Horizon 2020 research and innovation programme and Germany, Slovakia, The Netherlands, Spain, Italy. This work is also partially supported by the China Scholarship Council (CSC).

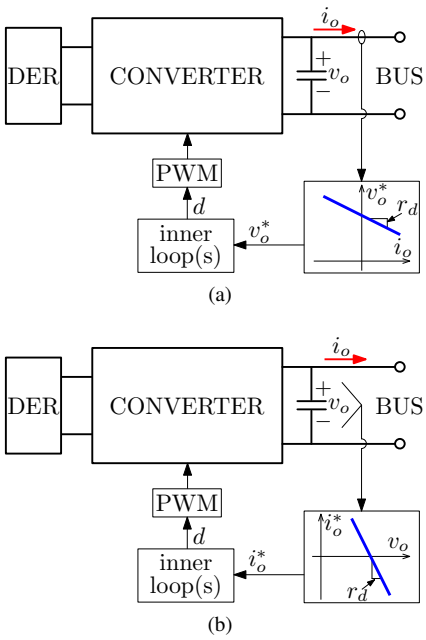

Figure 2. Droop-controlled DERs converters. (a) *V-I* droop; (b) *I-V* droop.

Although droop control provides a satisfactory strategy for nanogrids, additional enhancements are needed to achieve optimal operation. For instance, when a dc nanogrid is connected to an upstream grid, that is, in grid-connected mode, it is possible for DERs converters to utilize the droop control [5]. The drawback of doing this is obvious: DERs converters do not have the freedom of regulating their output power. Instead, the output powers are determined by the load consumption and the droop functions. In grid-connected mode, DERs converters are expected to operate with power flow control rather than droop control. In this way, renewable energy sources can maximize their output power, and energy storage systems can charge or discharge to maintain energy stored in a reasonable level [6]. Unfortunately, another problem arises with this control approach. Once the dc nanogrid is disconnected from the upstream grid, that is, in islanded mode, DERs converters should take the responsibility of regulating the dc bus voltage, which means they need to switch from power flow control to bus voltage control. Usually, to ensure the stability of the nanogrid during the transition, this switch can rely on time-critical communications with other elements in the nanogrid, or it can be triggered by abnormal variations of the dc bus voltage [7]. However, these two approaches increase the system complexity and decrease reliability. Hence, it is necessary to develop a control approach which allows dc nanogrids to seamlessly disconnect from the upstream grids.

Plug and Play is one of the major features of dc nanogrids. Sources and loads can plug into the distribution grids at any time, bringing to continuous changes in the configuration and structure of the nanogrid. This, together with the possibility of operating grid-connected or autonomously, poses relevant challenges in system stability [8]. In this context, on-line estimates of the converters stability margins can be effectively exploited for monitoring purposes and to tune the converters controllers, thus ensuring a more reliable operation [9].

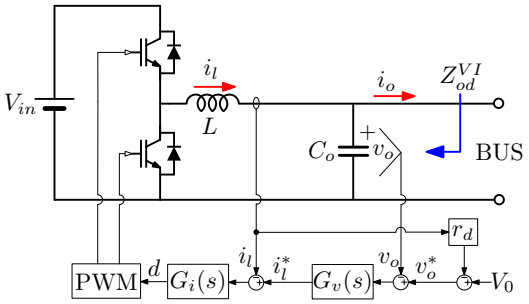

Figure 3. Control scheme of an example *V-I* droop-controlled converter.

This paper reviews the control approaches for dc-dc converters in dc nanogrids to stress the feature of *plug and play*. The similarity and difference between two different implementation methods of droop control are explored. Auxiliary functions, like seamless transition between different operation modes and on-line stability monitoring, are also introduced for the converters.

II. Implementations of Droop Control

Droop control is widely used to operate parallel connected converters in nanogrids. It can be regarded as the basis for other advanced control techniques. The implementation methods of droop control strategy can be categorized into two types: voltage-current (*V-I*) droop and current-voltage (*I-V*) droop, as shown in Fig. 2. The *V-I* droop method generates the output voltage reference v_o^* based on the sampled output current i_o and the droop coefficient r_d, which is typically designed as a constant:

$$v_o^* = V_0 - i_o \cdot r_d \tag{1}$$

where V_0 is the voltage set point at no load condition. On the other hand, The *I-V* droop control calculates the output current reference i_o^* according to the measured output voltage v_o and the droop coefficient r_d. The droop function is shown below:

$$i_o^* = \frac{V_0 - v_o}{r_d} \tag{2}$$

A buck converter is used as an example to better explain the characteristics of these two droop methods. The system parameters are reported in Table I.

A. V-I droop control

The control scheme of the *V-I* droop-controlled converter is shown in Fig. 3. The system parameters in this example are reported in Table I. It can be found that the *V-I* droop controller consists of an inductor current loop, an output voltage loop, and a droop loop. Regarding the controller design, generally, the current loop is designed at first, the voltage loop is then considered. Finally, the droop loop is closed. PI controllers are usually used for current regulator $G_i(s)$ and voltage regulator $G_v(s)$ to achieve zero dc steady-state errors.

Table I
SYSTEM PARAMETERS

Parameter	Symbol	Value
Input voltage	V_{in}	650 V
Nominal bus voltage	V_o	380 V
Nominal power	P_n	5 kW
Inductance	L	1.6 mH
Output capacitance	C_o	105 µF
Switching frequency	f_s	25 kHz
Voltage set point	V_0	380 V
Droop resistance	r_d	1.52 V/A

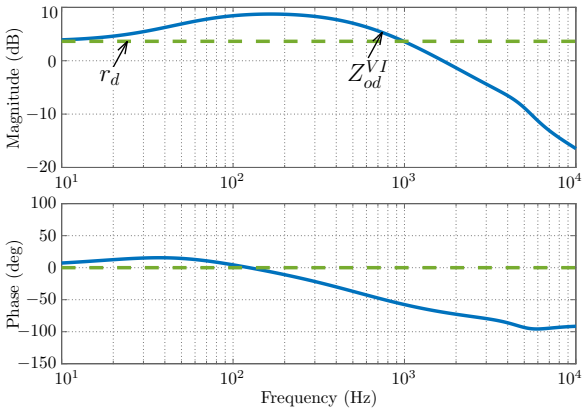

Figure 4. Bode diagram of the output impedance Z_{od}^{VI}.

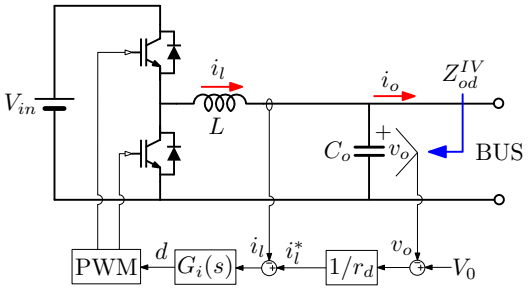

Figure 5. Control scheme of an example *I-V* droop-controlled converter.

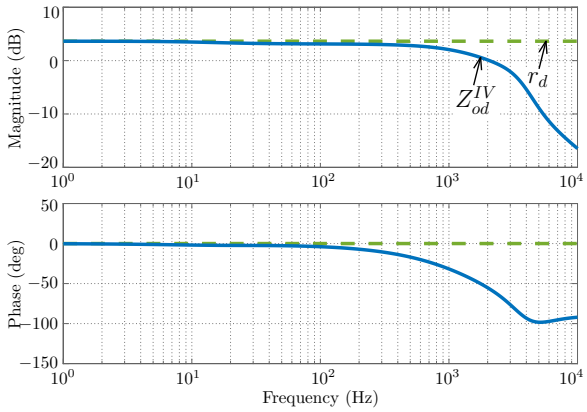

Figure 6. Bode diagram of the output impedance Z_{od}^{IV}.

To evaluate the steady-state and dynamic performances of this converter, its output impedance Z_{od}^{VI}, which reflects the output voltage fluctuations during load changes, is analyzed. By designing the current loop bandwidth and the voltage loop bandwidth at 2 kHz and 1 kHz respectively, the resulting output impedance Z_{od}^{VI} is depicted in Fig. 4. As can be seen, Z_{od}^{VI} is equal to the droop coefficient r_d in the low frequency range. Then, its magnitude becomes higher than r_d in the frequency range from 10 Hz to 1 kHz. In the high frequency range, Z_{od}^{VI} is dominated by the output capacitance. Further, it can be inferred that the bus voltage would show a significant undershoot or overshoot when having a step up or step down in load. To reduce the voltage undershoot/overshoot, the *V-I* droop controller needs to be improved or the output capacitance should be increased.

B. I-V droop control

The *I-V* droop controller is applied to the same buck converter and the control scheme is presented in Fig. 5. Compared to the *V-I* droop controller, the *I-V* droop controller removes the output voltage control loop, thus resulting in a simpler control structure.

The bode diagram of the output impedance Z_{od}^{IV} is given in Fig. 6. In the low frequency range, Z_{od}^{IV} is also equal to the droop coefficient r_d, which means the same steady-state performance as the *V-I* droop controller. Differently, the magnitude of Z_{od}^{IV} is always below r_d in the high frequency range. As a consequence, the *I-V* droop-controlled converter regulates its output voltage without any undershoot or overshoot during load changes. From this standpoint, the *I-V* droop control outperforms the *V-I* droop control.

III. ON-LINE STABILITY MONITORING TOOL

The on-line stability monitoring of a generic control loop of an electronic power converter in dc nanogrids applications is investigated in [9]. This approach is an extension of the Middlebrook's injection technique [10] to digitally-controlled switch-mode power converters. The technique consists in injecting a small-signal perturbation with given frequency into the control loop under study and measuring the loop gain at that frequency. As shown in Fig. 7, the digital controller implementation including, in particular, an analog-to-digital converter (ADC), a discrete-time compensator, and a digital pulse width modulator (DPWM) is considered for this application.

By referring to Fig. 7, the loop gain evaluated at $\tilde{f}$ is:

$$T(s)|_{s=j2\pi\tilde{f}} = -\left.\frac{s_y(s)}{s_x(s)}\right|_{s=j2\pi\tilde{f}} = -\frac{s_y(j\,2\pi\tilde{f})}{s_x(j\,2\pi\tilde{f})}, \quad (3)$$

where s_x and s_y are respectively the signals after and before injection point. By definition, the crossover frequency f_c of the control loop corresponds to the frequency $\tilde{f}$ of the perturbation signal at which the open-loop transfer function shows unity gain, while the phase margin PM is the phase shift between $s_x(j2\pi\tilde{f})$ and $s_y(j2\pi\tilde{f})$. That is, if:

$$|T(j\,2\pi\tilde{f})| = 1. \quad (4)$$

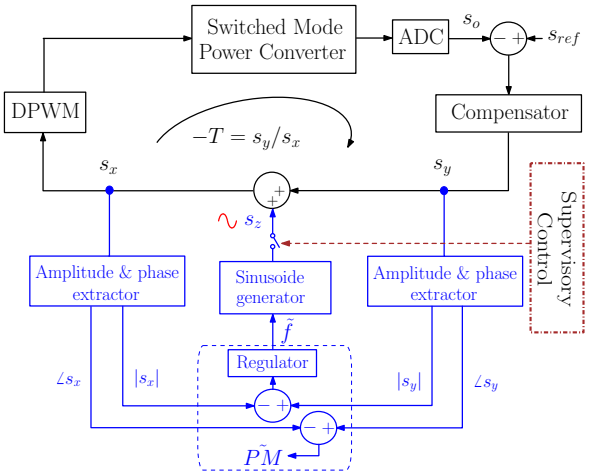

Figure 7. On-line stability monitoring for digitally-controlled converters (a generic control loop).

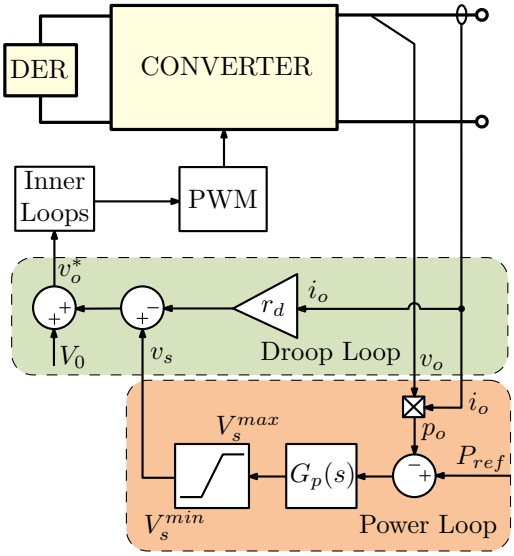

Figure 8. Scheme of the power-based droop control.

then: $f_c = \tilde{f}$ and $PM = \tilde{PM} = 180° + \angle T(j\,2\pi\tilde{f}) = \angle s_y(j\,2\pi\tilde{f}) - \angle s_x(j\,2\pi\tilde{f})$, where $\tilde{PM}$ indicates the estimated phase margin.

Thus, as shown in Fig. 7, the principle of the proposed crossover frequency and phase-margin estimation technique is to extract the amplitudes and the phases of signals s_x, s_y, and then to adjust the frequency $\tilde{f}$ of the injected perturbation s_z, by means of a PI regulator, in such a way that the amplitude difference between the two signals converges to zero (i.e., $|s_y| - |s_x| = 0$). In such an operating point, (4) holds. Therefore, the frequency $\tilde{f}$ and the phase shift $\angle s_y - \angle s_x$ are monitored as the crossover frequency and the phase margin of the considered control loop, respectively. The simple signal processing proposed to extract the magnitudes and phase of the two signal s_x, s_y is detailed in [9].

It is worth remarking that the amplitude of the injected small-signal perturbation should be set in such a way that the effects in the output currents and voltages due to the perturbation injection can be well tolerable (e.g., with respect to the rated values). The information obtained by the monitoring process may eventually be exploited to perform provisions that keep the loop under investigation far from instability (e.g., by auto-tuning the associated regulators).

IV. Power-based droop control

As discussed in Sec. I, a controller which is able to seamlessly switch from power flow control to droop control is needed. On the basis of the widely adopted *V-I* droop control block, a power-based droop controller is proposed for DERs converters to fulfill this target [11].

A. Control scheme

Fig. 8 shows the scheme of this control approach. Compared to the *V-I* droop controller shown in Fig. 2a, the power-based droop controller includes an external bounded power loop. The corresponding droop function can be expressed as:

$$\begin{aligned} v_o^* &= V_0 - r_d \cdot i_o + v_s \\ &= V_0 - r_d \cdot i_o + (P_{ref} - p_o) \cdot G_p(s) \end{aligned} \tag{5}$$

where v_s is the output of the power loop, P_{ref} is a given power reference, which can be generated according to the status of the DERs or can be determined by the nanogrid supervisor using non-critical communication, p_o is the output power, and $G_p(s)$ is the power regulator employed to regulate to zero the error $(P_{ref} - p_o)$. It should be noted that v_s has an upper saturation level V_s^{max} and a lower saturation level V_s^{min}. The idea behind this scheme is to add an addition degree of freedom, that is, v_s, to the controller to increase control flexibility. Thanks to this modification, as long as v_s is not saturated, the converter exactly tracks its given power reference P_{ref} in steady-state, while preserving all the merits of the conventional droop control if operating isolated from a stiff voltage source (e.g., a stronge GIC).

B. Operation modes

The operation modes of a single DERs converter implementing the power-based droop control can be classified into *power regulation mode* and *bus regulation mode*.

1) Power regulation mode: occurs when the output power p_o of a DERs converter exactly follows its reference P_{ref}, while the bus voltage is imposed (e.g., by other converters, like the GIC). In this operation mode, local power needs can be fulfilled by acting on P_{ref}; for example, local renewable sources can operate at their maximum power points, local storage can exchange power to restore a particular state-of-charge (SoC).

2) Bus regulation mode: occurs when a DERs converter takes charge of bus voltage regulation, while losing control

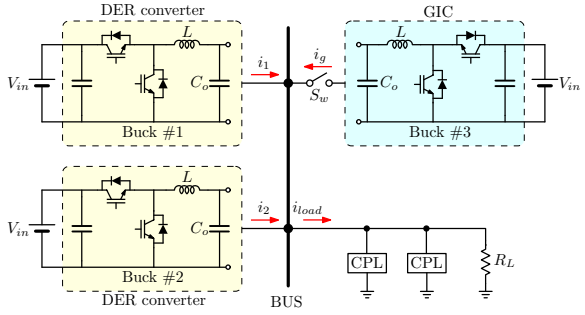

Figure 9. Schematic of the laboratory-scale dc nanogrid prototype.

Table II
EXPERIMENTAL SYSTEM PARAMETERS

Parameter	Symbol	Value
Converters		
Input voltage	V_{in}	380 V
Nominal bus voltage	V_{bus}	200 V
Nominal power	P_n	3 kW
Inductance	L_{in}	1.6 mH
Output capacitance	C_o	160 µF
Switching frequency	f_{sw}	12.5 kHz
Droop Loop		
Voltage set point	V_0	200 V
Droop coefficient	r_d	0.67 V/A
Power Loop		
Upper saturation level	V_s^{max}	10 V
Lower saturation level	V_s^{min}	−10 V

of its output power, turning actually into a traditional droop-controlled source. In this mode, the converter aims at balancing the power within the nanogrid, then, its output power p_o is, in general, not equal to the given power reference P_{ref} and the power loop saturates (i.e., v_s is kept at its maximum or minimum level).

3) Mode transitions: from the power regulation to the bus regulation mode occur, for example, due to faults on the upstream grid. In this situation, under the effect of the power loop, v_s deviates from its original steady-state value. Once v_s hits the saturation level, the controller degenerates to a traditional droop controller and operates in bus regulation mode. In this way, mode transitions are achieved seamlessly.

V. EXPERIMENTAL VERIFICATION

Fig. 9 shows the schematic of a laboratory-scale dc nanogrid prototype. The setup is composed of three equal converters. System parameters are listed in Table II.

A. Test of different droop control implementation methods

The steady-state and dynamic performances of the *V-I* droop control and *I-V* droop control now considered and compared.

Firstly, the *V-I* droop control shown in Fig. 3 is implemented on converter #1 and #2, and the GIC is disconnected from the grid. The current loop and the voltage loop bandwidths are designed equal to 1 kHz and 300 Hz, respectively. The transient corresponding to a load step is presented in Fig. 10. The bus voltage shows a large undershoot (2 V) during the transient and stabilizes 2.7-V below in steady state. Then, the *I-V* droop control shown in Fig. 5 is applied to converter #1 and #2. The results obtained considering the same load step change are shown in Fig. 11. Compared with the results of the *V-I* droop control, the bus voltage shows the same drop in steady state, but significantly less undershoot (0.4 V) during the transient. These experimental results relate to the analysis presented in Sec. II.

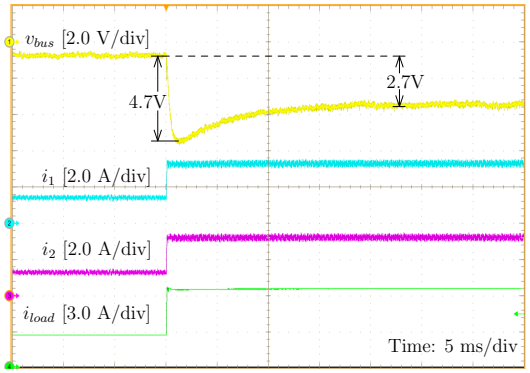

Figure 10. Transient response of *V-I* droop-controlled converters under a load change. v_{bus} offset: 200 V.

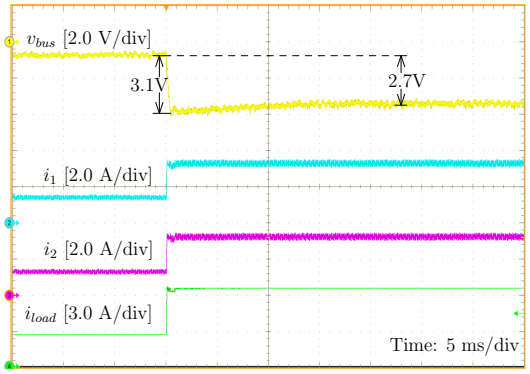

Figure 11. Transient response of *I-V* droop-controlled converters under a load change. v_{bus} offset: 200 V.

B. Test of the power-based droop control

The performance of the power-based droop control is tested under different operation modes, as well as during the modes transition process. Converter #1 and #2 employ the power-based droop control method, while the GIC operates as a constant voltage source.

When the GIC performs normally, converter #1 and #2 operate with power flow control. A power reference step change from 0 kW to 1 kW is applied to converter #1. The resulting dynamic performance is displayed in Fig. 12. The output current i_1 rises smoothly from 0 A to 5 A, with the delivered output power correspondingly increasing up to 1 kW. Accordingly, i_g reduces by 5 A to maintain the power balance.

The transition process is triggered by the opening of the switch S_w, that is, the disconnection of the GIC. The acquisition in Fig. 13 shows a smooth transient of the converters from the power flow control to the droop control. As a result, the

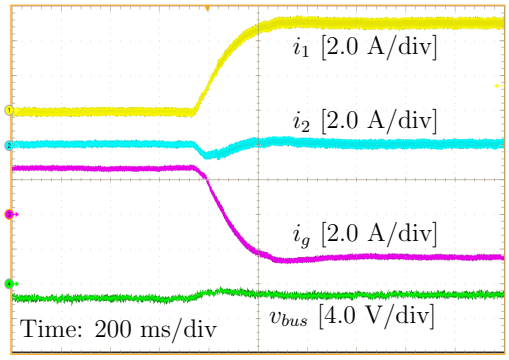

Figure 12. Transient response of P_{ref_1} step: 0 kW $\rightarrow$ 1 kW, with the GIC operating with constant voltage control. $P_{ref_2} = 0$ kW. v_{bus} offset: 200 V.

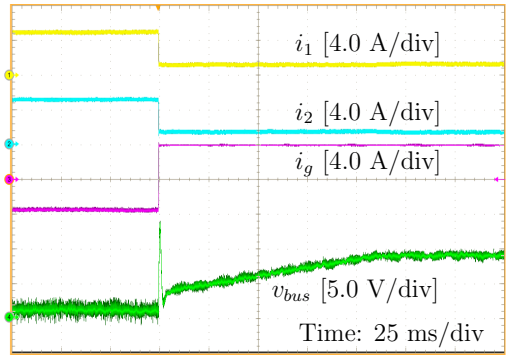

Figure 13. Transition process of the seamless disconnection of the GIC. $P_{ref_1} = 1$ kW and $P_{ref_2} = 1$ kW. i_g offset: -4 A, v_{bus} offset: 200 V.

nanogrid seamlessly transits from the grid-connected mode to the islanded mode. This shows the effectiveness of the power-based droop control method while transiting between modes.

A load step is applied while the GIC is disconnected. Converter #1 and #2 operate with droop control before and after the load step. The total load power is increased by 800 W, consequently, each DERs converter outputs 400 W more, that is, about 2 A of output current each. The bus voltage decreases by 1.4 V due to the droop function.

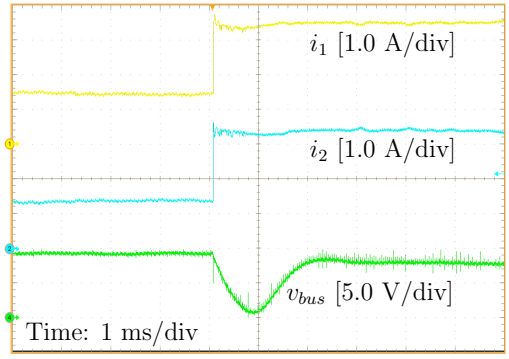

Figure 14. Transient response of load step with the GIC disconnected. $P_{ref_1} = 1$ kW and $P_{ref_2} = 1$ kW. v_{bus} offset: 200 V.

VI. Conclusion

This work presents an architecture of dc nanogrids and some state-of-the-art techniques to coordinate the contributions from the available distributed energy resources (DERs), featuring plug-and-play operation and enhanced stability. Typically, the droop control is employed to attain a natural repartition of the power needs among the converters interfacing the DERs to the dc distribution bus. Two main classes of droop control are revised and analyzed, namely, the *I-V* droop and the *V-I* droop. The *I-V* droop control is proven to have much less voltage overshoot/undershoot than the *V-I* droop control during load changes. Besides, droop controllers can be modified to have more control flexibility. The power-based droop controller is presented to enable power flow control in grid-connected mode and seamless transitions from the grid-connected operation to the islanded operation. On-line stability monitoring tools to be applied to the most critical control loops are contemplated to acquire useful information about the stability of the converters populating the nanogrid. Experimental results from a laboratory-scale dc nanogrid prototype are reported to show the operation and the feasibility of the discussed methods.

References

[1] R. H. Lasseter, "Microgrids," in *2002 IEEE Power Engineering Society Winter Meeting. Conference Proceedings (Cat. No.02CH37309)*, vol. 1, 2002, pp. 305–308 vol.1.

[2] D. Boroyevich, I. Cvetković, D. Dong, R. Burgos, F. Wang, and F. Lee, "Future electronic power distribution systems a contemplative view," in *2010 12th International Conference on Optimization of Electrical and Electronic Equipment*, May 2010, pp. 1369–1380.

[3] J. M. Guerrero, J. C. Vasquez, J. Matas, L. G. de Vicuna, and M. Castilla, "Hierarchical control of droop-controlled ac and dc microgrids – a general approach toward standardization," *IEEE Transactions on Industrial Electronics*, vol. 58, no. 1, pp. 158–172, Jan 2011.

[4] F. Gao, S. Bozhko, A. Costabeber, C. Patel, P. Wheeler, C. I. Hill, and G. Asher, "Comparative stability analysis of droop control approaches in voltage-source-converter-based dc microgrids," *IEEE Transactions on Power Electronics*, vol. 32, no. 3, pp. 2395–2415, March 2017.

[5] I. Cvetkovic, D. Dong, W. Zhang, L. Jiang, D. Boroyevich, F. C. Lee, and P. Mattavelli, "A testbed for experimental validation of a low-voltage dc nanogrid for buildings," in *2012 15th International Power Electronics and Motion Control Conference (EPE/PEMC)*, Sept 2012, pp. LS7c.5–1–LS7c.5–8.

[6] L. Xu and D. Chen, "Control and operation of a dc microgrid with variable generation and energy storage," *IEEE Transactions on Power Delivery*, vol. 26, no. 4, pp. 2513–2522, Oct 2011.

[7] F. Nejabatkhah and Y. W. Li, "Overview of power management strategies of hybrid ac/dc microgrid," *IEEE Transactions on Power Electronics*, vol. 30, no. 12, pp. 7072–7089, Dec 2015.

[8] A. Riccobono, M. Cupelli, A. Monti, E. Santi, T. Roinila, H. Abdollahi, S. Arrua, and R. A. Dougal, "Stability of shipboard dc power distribution: Online impedance-based systems methods," *IEEE Electrification Magazine*, vol. 5, no. 3, pp. 55–67, 2017.

[9] A. Khodamoradi, G. Liu, P. Mattavelli, T. Caldognetto, and P. Magnone, "On-line stability monitoring for power converters in dc microgrids," in *2017 IEEE Second International Conference on DC Microgrids (ICDCM)*, June 2017, pp. 302–308.

[10] R. D. Middlebrook, "Measurement of loop gain in feedback systems," *International Journal of Electronics Theoretical and Experimental*, vol. 38, no. 4, pp. 485–512, 1975.

[11] G. Liu, T. Caldognetto, P. Mattavelli, and P. Magnone, "Power-based droop control in dc microgrids enabling seamless disconnection from upstream grids," *IEEE Transactions on Power Electronics*, 2018.